Appl Phys A (2013) 113:355–359
DOI 10.1007/s00339-013-7635-1

Applied Physics A
Materials Science & Processing

Influence of the liquid environment on the products formed from the laser ablation of tin

O.R. Musaev · M.S. Driver · E.A. Sutter · A.N. Caruso · J.M. Wrobel · M.B. Kruger

Received: 2 October 2012 / Accepted: 13 February 2013 / Published online: 22 February 2013

Abstract Tin targets immersed in ethanol and distilled water were ablated using a UV pulsed laser. The ablated products were investigated with transmission and scanning electron microscopy, X-ray photoelectron spectroscopy, and energy dispersive spectroscopy. For ablation in both liquids, the size distribution of the produced particles was bimodal, with particles having diameters of ∼10 nm and ∼1 μm. Formation mechanisms that caused the bimodal distribution are suggested. Ablation in ethanol resulted in nanoparticles that were found to be single crystals of tin coated with tin hydroxide ($Sn(OH)_2$) while ablation in water yielded nanoparticles that were polycrystalline tin dioxide (SnO_2) throughout.

1 Introduction

Laser ablation in liquids is an easily implemented method, which can be used to fabricate nanoparticles and offers advantages over other techniques [1–3]. This versatile approach to nanoparticle fabrication has been used to form metallic, dielectric, and semiconducting nanoparticles of both elements and compounds and is used commercially for nanoparticle production [4–12]. In addition to laser wavelength, fluence, and pulse duration, the liquid in which the target is immersed offers another parameter to be changed to allow for the selection of nanoparticles with desirable properties. For example, the addition of surfactants can result in smaller sizes of particles because of less efficient agglomeration [10, 13]. Additionally, the shape of the produced nanoparticles can be altered by the introduction of an external electric field [14]. Ablation in liquids, as compared to vacuum can result in chemical reactions and long range physical structures; some very unique because of the state of the ablated material and the ability to rapidly quench [15, 16].

Tin is an important technological material that finds applications as a catalyst, a coating preventing oxidation, and is a component of solders for the electronics industry [17, 18]. Tin oxide nanoparticles are used for oxygen sensing applications [19, 20] while tin nanoparticles were used for development of highly conductive ink [21] and have been used for fabrication of anode composite materials in high efficiency Li based batteries [22, 23]. Sn nanoparticles have previously been synthesized via chemical and physical methods [18, 24, 25]. They were also fabricated by laser ablation with 5 ns pulses of 532 nm light in water, acetone, and ethanol [26]. Laser fluence and the liquid affected the size distribution, although the produced particles had sizes that clustered around a single size from 5 to 40 nm.

In this paper, we report fabrication of nano and micron scale particles by laser ablation of Sn targets in two different liquids, water and ethanol. Scanning electron microscopy (SEM) and TEM images were taken to analyze the morphologies and sizes of the obtained particles. Electron diffraction was used to determine the composition and structure of the nanoparticles, while X-ray photoelectron spectroscopy (XPS) was used to determine the chemical composition of their surface.

O.R. Musaev (✉) · M.S. Driver · A.N. Caruso · J.M. Wrobel · M.B. Kruger
Department of Physics and Astronomy, University of Missouri Kansas City, 5110 Rockhill Rd., Kansas City, MO 64110, USA
e-mail: musaevo@umkc.edu
Fax: +1-816-2355221

E.A. Sutter
Center for Functional Nanomaterials, Brookhaven National Laboratory, Upton, NY 11973, USA

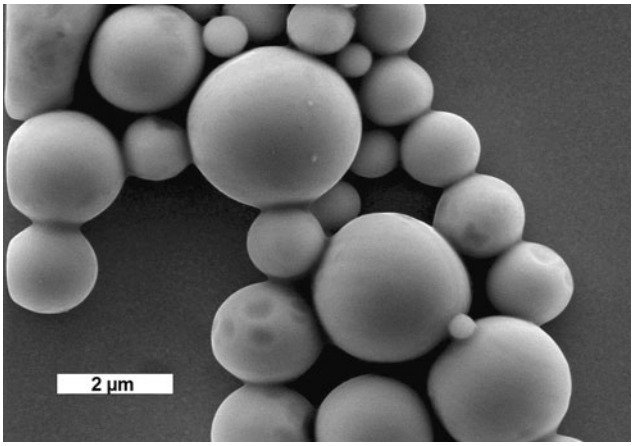

Fig. 1 SEM image of micron sized particles formed from ablation in alcohol

2 Experimental

A tin target was immersed in either ethanol or distilled water, at room temperature, and ablated with UV pulsed nitrogen laser radiation with 10 nm pulse duration having a wavelength of 337 nm and a repetition rate of 10 Hz. The laser beam was focused by a silica lens with a focal length of 9.5 cm onto the surface of the target resulting in a fluence of ∼50 J/cm^2. The target was placed approximately 2 cm below the surface of the liquid. After formation of a colloidal solution, a piece of gold coated Si wafer was placed at the bottom of the beaker containing the colloid. The beaker was then positioned under a hood to allow for evaporation of the liquid. The ablated product deposited on the wafer was subsequently investigated by SEM and XPS. For TEM, the same procedure was used to place the particles on a carbon-coated copper grid. SEM micrographs were obtained with a Philips SEM 515 scanning electron microscope equipped with an energy dispersive spectroscopy (EDS) system that included an IMIX-PC energy dispersive spectrometer with a Prism (Princeton Gamma-Tech) detector. TEM images and electron diffraction patterns were obtained using a JEOL 2100F field-emission microscope. A Kratos Axis HS was used to collect the XPS spectra. Al K_α X-rays (1486.7 eV) were used to investigate the chemical composition of the surface of the ablated products, in angle integrated mode with charge balance applied.

3 Results and discussion

Ablation in alcohol resulted in particles that fall within one of two different size regimes. An SEM image of micron-sized particles is shown in Fig. 1. All of the particles are spherical with diameters varying from 0.2 to 2 µm. A TEM image of nanosize particles, which have an upper size of

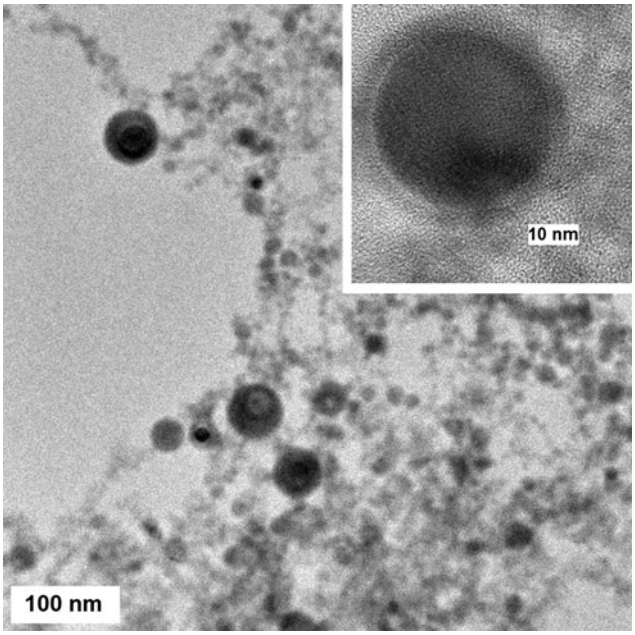

Fig. 2 TEM image of ∼10 nm sized particles formed from ablation in alcohol. The *insert* is an HRTEM image of a single nanoparticle

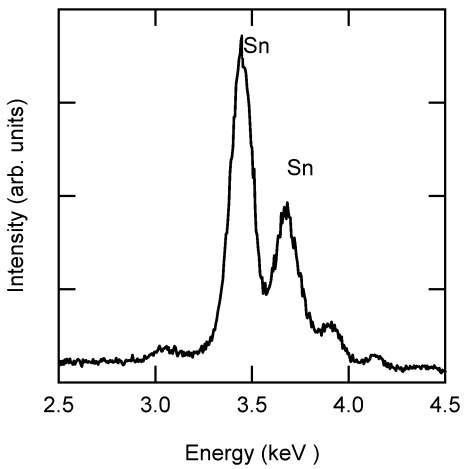

Fig. 3 EDS spectrum of products ablated in alcohol that were deposited on a gold coated silicon wafer

∼30 nm, is shown in Fig. 2 along with a HRTEM image in the insert. The nanoparticle shown in the insert is covered by a carbon rich layer most likely resulting from decomposition of alcohol, which is common to all of the particles formed from ablation in alcohol and studied using HRTEM. An EDS spectrum collected during SEM imaging of the ablated product (Fig. 3) is dominated by two Sn peaks confirming the presence of this element in the nanoparticles. The electron diffraction pattern from an individual 30 nm particle is shown in Fig. 4. It shows sharp spots and faint diffuse rings. The rings stem from the carbon support film on which the particles are spread. The sharp spots can be indexed to tetragonal β-Sn [27]. The circles, labeled with indices, indi-

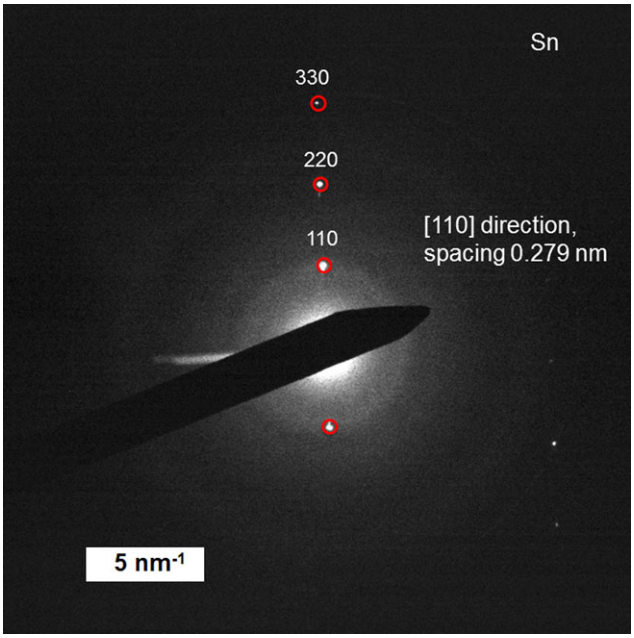

Fig. 4 Electron diffraction pattern of nanoparticles obtained in alcohol. *Circles* and *Miller indices* on the image indicate crystallographic planes of Sn

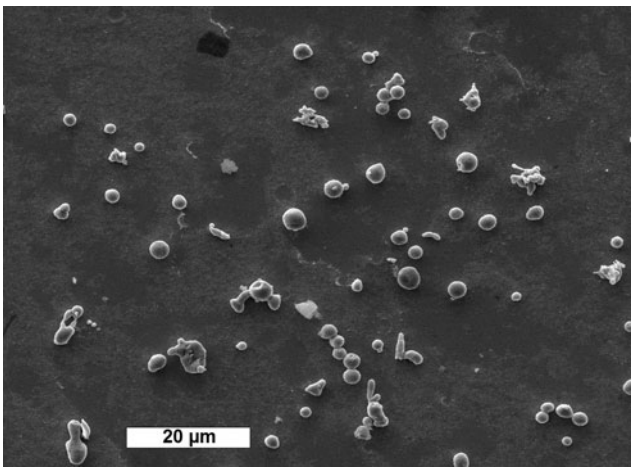

Fig. 5 SEM image of micron sized particles formed by ablation in water

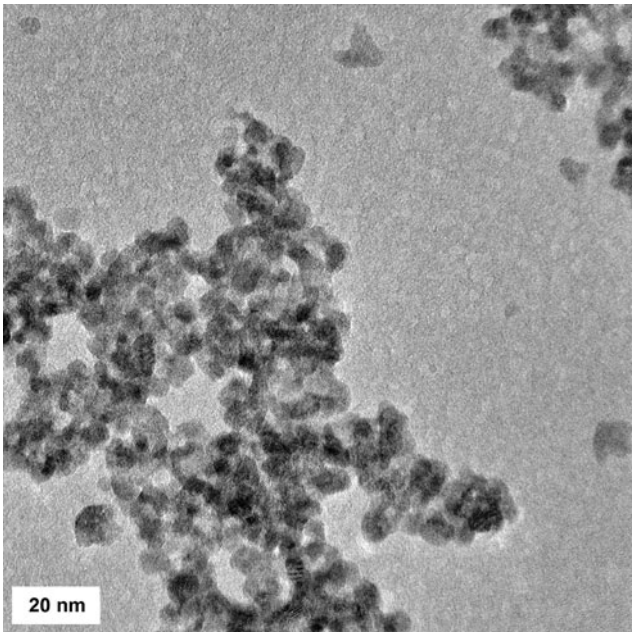

Fig. 6 TEM image of ∼10 nm sized particles formed by ablation in water

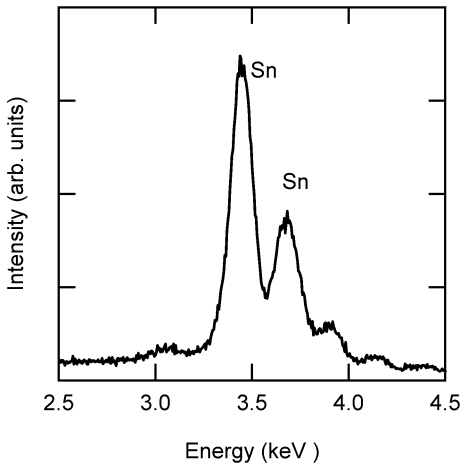

Fig. 7 EDS spectrum of products ablated in water that were deposited on a gold coated silicon wafer

cate the simulated reflections for a single crystal of Sn. The excellent agreement demonstrates that the nanoparticle is a single crystal of tin.

Ablation in water also resulted in particles with two different size regimes. Figure 5 is an SEM image of particles with diameters in the micron-size range. While the size of these large particles is similar to those formed in alcohol, the morphologies differ. Large particles formed in ethanol look smoother and have a more regular spherical shape than the particles formed in water. A TEM image of nanosize particles, which have an upper size of ∼30 nm, is shown in Fig. 6. The two peaks observed in the EDS spectrum (Fig. 7), which was collected during SEM imaging, demonstrate that the particles contain tin. Figure 8 is an electron diffraction pattern from an individual 30 nm particle. It consists of rings indicating that the particles are polycrystalline. Although the diffraction pattern cannot be indexed to any Sn structure, it can be indexed to tetragonal SnO_2 [28].

XPS studies were performed on the ablated products to compare how the liquid environment affects the structure and composition of the particles' surfaces. The XPS spectra, which are shown in Fig. 9, demonstrate there are different chemical compositions at the surfaces of the particles made in ethanol and water. Metallic Sn has two core level peaks, the $3d_{5/2}$ at 484.65 eV, and the $3d_{3/2}$ peak at

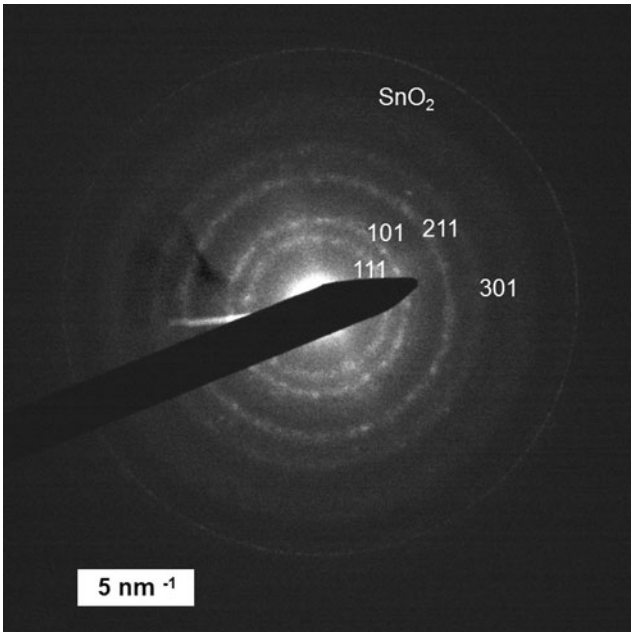

Fig. 8 Electron diffraction pattern from nanoparticles formed in water

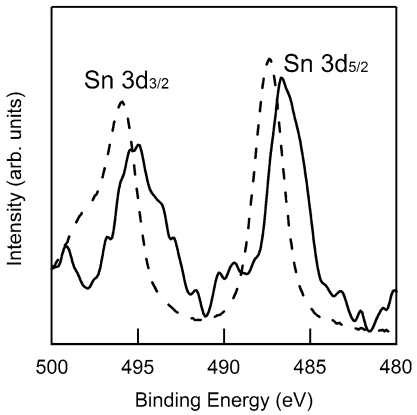

Fig. 9 XPS spectra of particles fabricated by ablation in alcohol (*solid*) and water (*dashed*)

493.15 eV [29, 30]. The spectra from particles ablated in water and those ablated in ethanol are shifted relative to the spectrum of Sn^{0+} and also to one another. The spectrum of the ethanol-ablated Sn has peaks in the vicinity of 486.7 eV and 495.0 eV, while the spectrum of water-ablated Sn has peaks at 487.4 eV and 495.9 eV. Based on literature comparisons, we have determined that the Sn ablated in ethanol yields particles covered with $Sn(OH)_2$ while the products ablated in water have a SnO_2 surface [31, 32].

Both water and ethanol resulted in the formation of round particles that fall into two size regimes, tens of nanometers and microns. Different mechanisms have been suggested to explain formation of the larger particles, those in the 0.1 μm to 1 μm range. These include spallation (mechanical fragmentation), Rayleigh–Taylor instability, and Kelvin–Helmholtz instability [33–35]. Spallation is a plausible mechanism for femtosecond ablation because electrons in the surface are heated to much higher temperatures, with subsequent strong shock waves, in comparison with nanosecond pulses [33]. However, since electron-lattice relaxation time has a timescale of the order of ps this mechanism is less plausible for the 10 ns pulses used in this experiment. Kelvin–Helmholtz instability occurs due to velocity shear in liquids while Rayleigh–Taylor instability occurs at the interface of liquids with different densities [36]. Both instabilities were suggested to explain formation of droplets in the ablation process due to tangential motion of melted layers at moderate laser fluences [35, 37]. Numerical estimates for aluminum ablation with 20 ns 248 nm light and a fluence of 3 J/cm^2 give a droplet size of 50 nm due to Kelvin–Helmholtz instability. The Rayleigh–Taylor instability model under different scenarios gives estimates of micron scale particles only for multipulse irradiation at low or moderate fluences of nanosecond pulses. These models are not adequate for explaining micron scale particle formation for ∼10 J/cm^2 fluences and ∼10 ns pulse durations of highly absorbing materials because they do not take phase explosion into account [38].

We suggest that the double peak size distribution of particles is due to two physical mechanisms that occur during high intensity laser ablation: phase explosion [38, 39] and Rayleigh–Plateau hydrodynamic instability [36, 40]. During phase explosion, homogeneous nucleation in a metastable melt occurs when vapor bubbles form in the overheated liquid. This results in formation of particles with sizes of ∼10 nm from the vapor and liquid droplets in the plume [39].

The micron size particles are created in a different mechanism. During laser irradiation with a Gaussian beam, the target's surface temperature rises more quickly in the center. Phase explosion occurs in the center of the spot and a shockwave pushes the melted material radially outward. Rayleigh–Plateau instability of the melted jet likely results in the formation of the particles in the micron size range [40].

A kinetic model for formation of nanoparticles during laser ablation was developed and applied for nanodiamond fabrication by laser ablation of graphite in water [41]. In this model factors, such as rate of collisions between atoms, clusters and nanoparticles, adsorption energy for atoms, saturation pressure, and pressure and temperature of the plume, determine the final morphology of the nanoparticles. Chemical interactions with water were not included. In the case of ablation of tin in water, there is oxidation of the nanoparticles during phase explosion. The combination of growth and oxidation, which occurs in nonequilibrium conditions, may be the reason for the resulting polycrystalline particles. In contrast, there is evidently little chemical reaction between

the ablation products and alcohol. A plausible explanation for formation of single crystal nanoparticles in alcohol is that nanodroplets of tin melt formed in phase explosion have enough time to crystallize.

4 Conclusions

Tin targets were ablated in ethanol and water by a UV pulsed laser. Ablation in both liquids resulted in material that consisted of micron and nanometer scale particles. Diffraction patterns show that nanoparticles ablated in ethanol are single crystals of tin, while XPS spectra show they are coated with tin hydroxide. In contrast, ablation in water yields polycrystalline nanoparticles of tin oxide. These results demonstrate the ability to control the chemical composition of nanoparticles by changing the ablation environment. The observed bimodal size distribution of particles is explained by two different physical mechanisms of formation. Nanometer size particles are formed during phase explosion, while micron scale particles are due to Rayleigh–Plateau instability of the ejected melt.

Acknowledgements This work was partially supported by National Science Foundation Contracts DMR-0605493 and DMR-0923166 and was partially performed at the Center for Functional Nanomaterials, Brookhaven National Laboratory, under the auspices of the US Department of Energy, under Contract No. DE-AC02-98CH10886.

References

1. S. Besner, A.V. Kabashin, M. Meunier, Appl. Phys. A **88**, 269 (2007)
2. K.V. Anikin, N.N. Melnik, A.V. Simakin, G.A. Shafeev, V.V. Voronov, A.G. Vitukhnovsky, Chem. Phys. Lett. **366**, 357 (2002)
3. O.R. Musaev, V. Dusevich, D.M. Wieliczka, J.M. Wrobel, M.B. Kruger, J. Appl. Phys. **104**, 084316 (2008)
4. S. Arcidiacono, N.R. Bieri, D. Poulikakos, C.P. Grigoropoulos, Int. J. Multiph. Flow **30**, 979 (2004)
5. O.R. Musaev, J.M. Wrobel, D.M. Wieliczka, V. Dusevich, M.B. Kruger, Physica E **40**, 3147 (2008)
6. W.T. Nichols, T. Sasaki, N. Koshizaki, J. Appl. Phys. **100**, 114912 (2006)
7. G.W. Yang, Prog. Mater. Sci. **52**, 648 (2007)
8. H. Zeng, X.-W. Du, S.C. Singh, S.A. Kulinich, S. Yang, J. He, W. Cai, Adv. Funct. Mater. **22**, 1333 (2012)
9. O.R. Musaev, E.A. Sutter, J.M. Wrobel, M.B. Kruger, J. Nanopart. Res. **14**, 654 (2012)
10. D. Amans, C. Malaterre, M. Diouf, C. Mancini, F. Chaput, G. Ledoux, G. Breton, Y. Guillin, C. Dujardin, K. Masenelli-Varlot, P. Perriat, J. Phys. Chem. C **115**, 5131 (2011)
11. P. Liu, Z. Li, W. Cai, M. Fang, X. Luo, RSC Adv. **1**, 847 (2011)
12. W. Soliman, N. Takada, K. Sasaki, Appl. Phys. Express **3**, 035201 (2010)
13. F. Mafune, J. Kohno, Y. Takeda, T. Kondoh, H. Sawabe, J. Phys. Chem. B **105**, 5114 (2001)
14. P. Liu, H. Cui, C.X. Wang, G.W. Yang, Phys. Chem. Chem. Phys. **12**, 3942 (2010)
15. O.R. Musaev, A.E. Midgley, D.V.S. Muthu, J.M. Wrobel, M.B. Kruger, Mater. Lett. **63**, 893 (2009)
16. Z. Yan, R. Bao, C.Z. Dinu, Y. Huang, A.N. Caruso, D.B. Chrisey, J. Optoelectron. Adv. Mater. **12**, 437 (2010)
17. K. Fatih, R. Neagu, V. Alzate, V. Neburchilov, R. Maric, W. Haijiang, ACM Trans. Embed. Comput. Syst. **25**, 1117 (2009)
18. Y. Kwon, M.G. Kim, Y. Kim, Y. Lee, J. Cho, Electrochem. Solid-State Lett. **9**, A34 (2006)
19. G. Lu, L. Ocola, J. Chen, Adv. Mater. **21**, 2487 (2009)
20. R.W.J. Scott, S.M. Yang, N. Coombs, G.A. Ozin, D.E. Williams, Adv. Funct. Mater. **13**, 225 (2003)
21. Y.H. Jo, I. Jung, C.S. Choi, I. Kim, H.M. Lee, Nanotechnology **22**, 225701 (2011)
22. Y. Yu, L. Gu, C. Zhu, P.A. van Aken, J. Maier, J. Am. Chem. Soc. **131**, 15984 (2009)
23. W.-M. Zhang, J.-S. Hu, Y.-G. Guo, S.-F. Zheng, L.-S. Zhong, W.-G. Song, L.-J. Wan, Adv. Mater. **20**, 1160 (2008)
24. A. Caballero, J. Morales, L. Sanchez, Electrochem. Solid-State Lett. **8**, A464 (2005)
25. G. Cardenas, M. Melendrez, C. Cruzat, J. Diaz, Acta Microsc. **16**(Supp. 2), 135 (2007)
26. G. Bajaj, R.K. Soni, Appl. Phys. A **97**, 481 (2009)
27. V.T. Deshpande, D.B. Sirdeshmukh, Acta Crystallogr. **15**, 294 (1962)
28. W.H. Baur, A.A. Khan, Acta Crystallogr., B Struct. Crystallogr. Cryst. Chem. **27**, 2133 (1971)
29. N. Faradzhev, V. Sidorkin, J. Vac. Sci. Technol. A **27**, 306 (2009)
30. C.D. Wagner, W.M. Riggs, L.E. Davis, J.F. Moulder, G.E. Mullenberg, *Handbook of X-Ray Photoelectron Spectroscopy*, Perkins-Elmer, Eden Prairie (1979)
31. S. Shukla, S. Seal, J. Akesson, R. Oder, R. Carter, Z. Rahman, Appl. Surf. Sci. **181**, 35 (2001)
32. M.S. Huh, B.S. Yang, J. Lee, J. Heo, S.J. Han, K. Yoon, S.-H. Yang, C.S. Hwang, H.J. Kim, Thin Solid Films **518**, 6343 (2009)
33. M.E. Povarnitsyn, T.E. Itina, M. Sentis, K.V. Khischenko, P.R. Levashov, Phys. Rev. B **75**, 235414 (2007)
34. R. Hergenröder, Spectrochim. Acta, Part B Atom. Spectrosc. **61**, 284 (2006)
35. A.B. Brailovsky, S.V. Gaponov, V.A. Luchin, Appl. Phys. A **61**, 81 (1995)
36. P.G. Drazin, W.H. Reid, *Hydrodynamic Stability* (Cambridge University Press, Cambridge, 1981)
37. D. Bäuerle, *Laser Processing and Chemistry*, 3rd edn. (Springer, Berlin, 2000)
38. A. Miotello, R. Kelly, Appl. Phys. Lett. **67**, 3535 (1995)
39. M.M. Martynyuk, Combust. Explos. Shock Waves **13**, 178 (1977)
40. W.A. Sirignano, C. Mehring, Prog. Energy Combust. Sci. **26**, 609 (2000)
41. C.X. Wang, P. Liu, H. Cui, G.W. Yang, Appl. Phys. Lett. **87**, 201913 (2005)